# 13
# Magnetisation excavation anomalies over the Tasmanian dolerites and application to magnetic modelling of small Martian impact craters

*C.A. Foss and J.R. Austin*

## ABSTRACT

Magnetic field variations arise due to contrasts in magnetisation. Where part of a sheet of magnetisation is removed in the excavation of valleys the resulting magnetic field variations can alternatively be modelled as due to the contrast of the remaining sheet against air or the contrast of air against the sheet. Where regions of removed magnetisation are localised there are advantages in modelling the volume from which magnetisation has been removed rather than the more extensive surrounding volume of remaining magnetisation. We present a model study of magnetisation excavated in valleys incised through volcanic sheets in south-east Tasmania and then apply the same methodology in a model emulation of magnetic fields over a Martian impact crater where crustal magnetisation has been excavated in an impact event. On Earth, where there are only limited exposures of homogeneous strongly magnetised rocks and where terrain is continually modified by surface processes, many impact craters have weak or complex magnetic field expressions. However, on Mars many small impacts into an igneous crust might better suit investigation of crustal magnetisation direction. The initial flights of NASA's Ingenuity with over 10 km of distance covered at heights of up to 20 m suggest that future developments may make feasible the measurement of magnetic profiles across minor terrain features. We show that it should be possible to recover magnetisation estimates from small impact craters even if there is associated demagnetisation beneath and around them.

## 13.1 INTRODUCTION

Magnetic field variations are mostly modelled as departures from a background field postulated to be the field that would be present if the investigated magnetisation was absent. In this chapter we investigate magnetic field variations that we consider due to contrasts between a zone from which magnetisation has been removed by excavation and an adjacent remaining magnetisation. These are specific cases of magnetisation deficit anomalies considered in the Chapter 12, in which a weak or non-existent magnetisation is surrounded by a stronger magnetisation. As discussed in Chapter 11, there are significant advantages in modelling terrain-related magnetisations because the known top surface of the magnetisation constrains estimation of other magnetisation parameters. Advantages of modelling excavated (missing) magnetisation are most evident where the excavations are of limited extent and the field needs only to be modelled to short distances

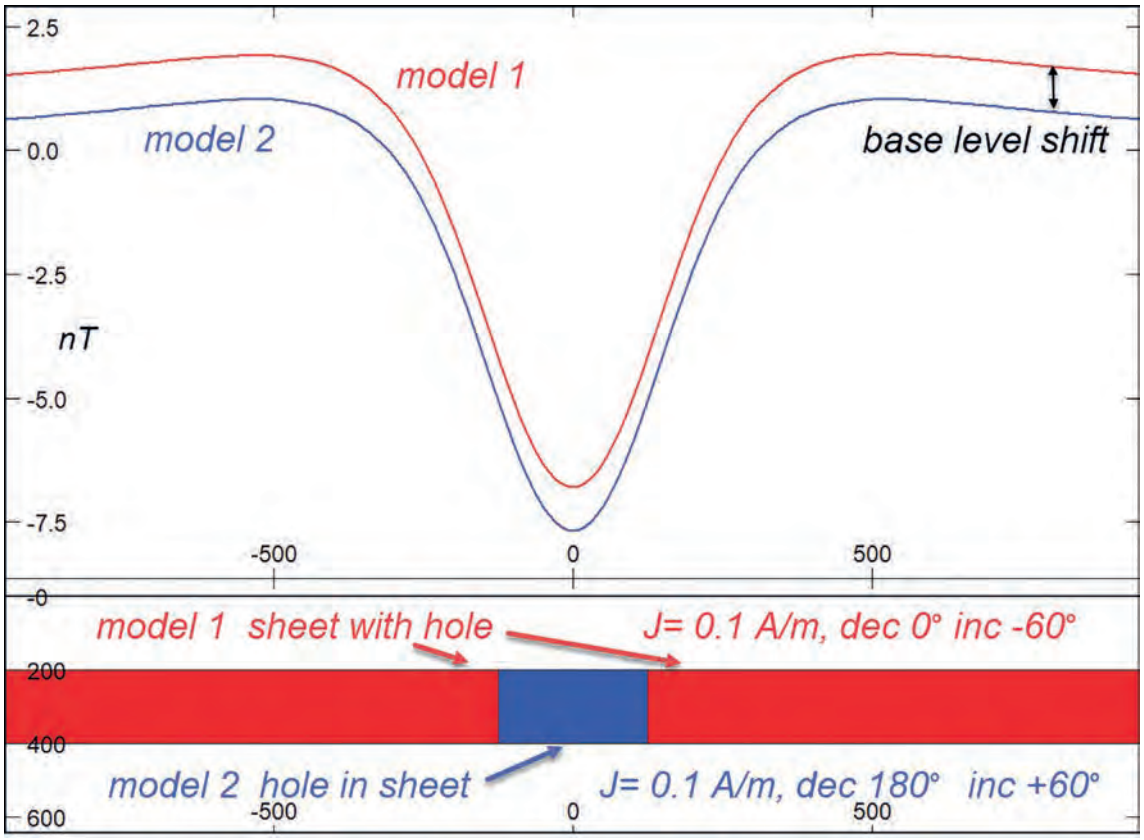


**Fig. 13.1.** East–west traverse in a 60° south magnetic field of a sheet with a gap in it (in red) and of an equal strength oppositely directed magnetisation occupying the gap (in blue).

away from their edges. The alternative of directly modelling the surrounding magnetisation requires either extending the model much further or facing concerns about edge-of-model termination artefacts extending into the region of interest. Two differences in modelling excavation magnetisations are in the background field levels and the apparent directions of magnetisation. In modelling an excavation magnetisation the magnetic field of the (estimated) complete sheet of magnetisation is included in the background field, and the excavation magnetisation has equal strength and anti-parallel direction to the magnetisation that has been removed.

Figure 13.1 shows the close equivalence between the magnetisation of a sheet with a gap in it and a magnetisation of equal strength and opposite direction occupying the gap. The difference between the two is the base shift due to the difference in magnetisation present in the two models. These different base levels have little significance in modelling or inversion of magnetic field data because the absolute value of the background field is unknown and is empirically set to the smoothed value of the field surrounding the variation of interest ('the regional field'). The issue of selecting the appropriate background field can be significantly reduced by modelling gradients rather than fields.

We investigated excavation anomalies over a sheet of Jurassic dolerite in south-east Tasmania where the sheets and valleys cut through them dominate the terrain and have associated sharp, high-amplitude magnetic field variations. The dolerites are part of the Antarctic-Australia Ferrar flood-basalt volcanism with trace element compositions that suggest crustal contamination of a mantle source (Brauns *et al*. 2000; Hergt and Brauns 2001). Leaman (2002) suggests a default effective susceptibility value of 0.07 SI for modelling magnetic field variations due to these rocks. Measured susceptibilities are highly variable with a mean of less than 0.02 SI (Leaman 2002) but remanent magnetisation is strong, with Koenigsberger ratios in some cases

greater than 10. The remanent magnetisation is mostly sub-parallel to the induced magnetisation or has slightly higher inclination, and stratigraphically lower zones of the dolerites include layers of reverse magnetisation. Jaeger and Joplin (1954) reported magnetisation of samples from borehole cores through several sheets, including one with an estimated thickness of 600 m. They found very variable intensity of magnetisation with steep inclinations and reversal towards the base of the sheet. Irving (1956, 1963) presented paleomagnetic NRM (natural remanent magnetisation) measurements from 30 dolerite sites in central to eastern Tasmania. The closest sampling site to our study area is site 28 that has a reported NRM direction of declination 68° and inclination −80° from two samples with an angular difference of 18°. A study by Schmidt (1976) extended sampling of the dolerites and included alternating field and thermal demagnetisation. These laboratory studies confirmed that the NRM directions measured on the dolerites are stable. A subsequent study by Schmidt and McDougall (1977) with both palaeomagnetic investigations and potassium-argon dating reconfirmed a split in magnetisation directions (including an anomalous easterly direction in our magnetic field study area) but found no systematic correlations between age and magnetisation direction.

We believe that there may be future opportunities to exploit excavation anomalies to estimate crustal magnetisations on Mars where impact craters of a wide range of sizes have excavated crustal material. Robbins and Hynek (2012) have created a database of over 384,000 craters with diameter > 1 km. Of these more than 300,000 have diameters < 3 km. There have been many studies of large Martian impact structures to investigate crustal-scale magnetisation that can be mapped at satellite elevations (Arkani-Hamed 2005; Shahnas and Arkani-Hamed 2007; Louzada *et al*. 2011; Lillis *et al*. 2013; Vervelidou *et al*. 2017). Reduction of magnetisation by excavation is further enhanced by the influence of shock demagnetisation in the rocks surrounding and beneath the craters. Demagnetisation effects depend on the unknown magnetic coercivity of the impacted crust, but Mohit and Arkani-Hamed (2004) and Shahnas and Arkani-Hamed (2007) suggest that at least for craters of several hundred kilometres diameter, demagnetisation may extend from the crater by as much as 80% of the crater radius. Demagnetisation is primarily due to shock effects with a secondary influence of thermal effects. Mittelholz *et al.* (2020) detected magnetic field variations on low-level MAVEN tracks close to a 35 km diameter crater in the region of Apollinaris Patera that include a reduction in the local magnetic field strength by 75%. They modelled the crater with a vertical cylindrical hole with surrounding demagnetisation extending the diameter by 50% and found that demagnetisation accounted for a reduction in magnetic field strength of 60%. However, we are primarily interested in smaller craters (including secondary craters formed by return of ejecta from a primary impact). Reliable mapping of the magnetic field signatures of these smaller craters of only several kilometres diameter or less are at or below resolution limits of the current satellite data but could be suitable for surface exploration by rovers or UAVs. For a vertical cylinder of vertical magnetisation contrast of 1 A/m and height to diameter ratio 0.1, the vertical magnetic field component $B_z$ is 400 nT at a clearance that is 10% of the cylinder height. At a clearance equal to the cylinder height $B_z$ falls to 150 nT. The scale independence of these magnetisation-plus-measurement distributions suggests that craters across a wide range of sizes might be suitable for magnetisation analysis.

## 13.2 MAGNETISATION EXCAVATION ANOMALIES IN SOUTH-EAST TASMANIA

Figure 13.2 shows the location of the Lost Falls Forest in south-east Tasmania. The East Tasmania Aeromagnetic and Radiometric Survey was flown over this area in 2022 for Mineral Resources Tasmania (MRT) on east–west flightlines at a spacing of 200 m. The data are available for download from the Geoscience Australia GADDS (Geophysical Archive Data Delivery System) as survey P5020. Figure 13.3 shows digital terrain elevation (DEM) and total magnetic intensity (TMI) images of part of the area. Much of the relief is due to thick sub-horizontal layers of basalt. Where rivers cut through these layers they incise deep and often steep-sided valleys. The magnetic field variation in the study area is over 2000 nT and the dendritic drainage pattern seen in the terrain image in Fig. 13.3A is also visible as magnetic lows in the TMI image in Fig. 13.2B. We selected the area outlined in Fig. 13.3 because it is a plateau of subdued elevation changes except where cut by valleys. The associated TMI image suggests that magnetisation is

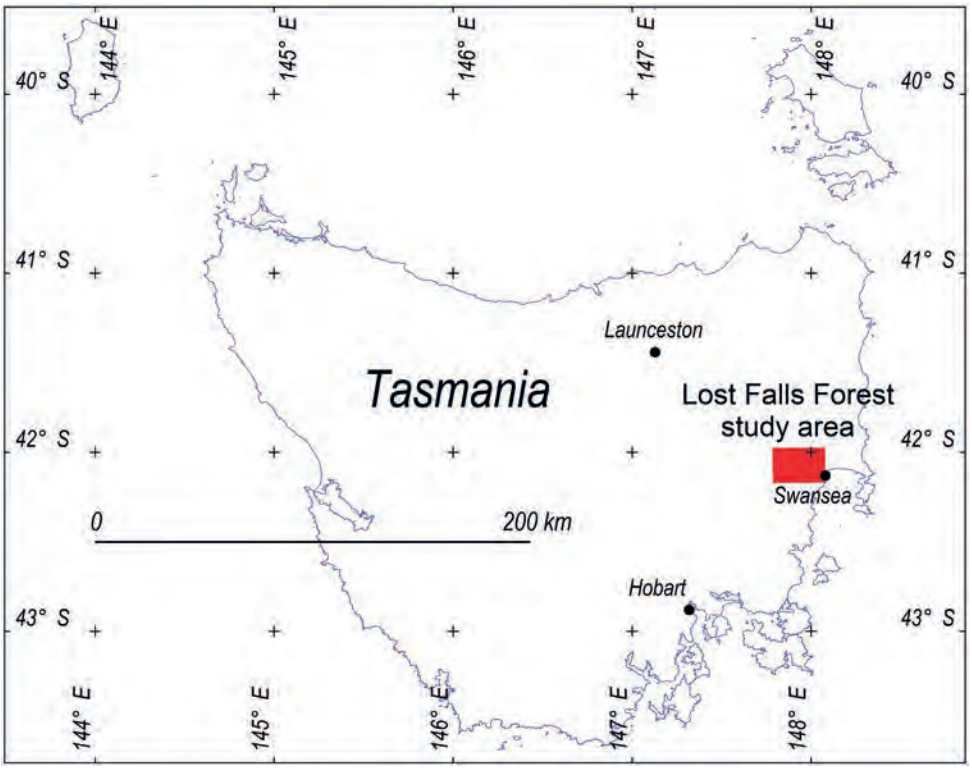


**Fig. 13.2.** Location of the Lost Falls Forest study area in south-east Tasmania.

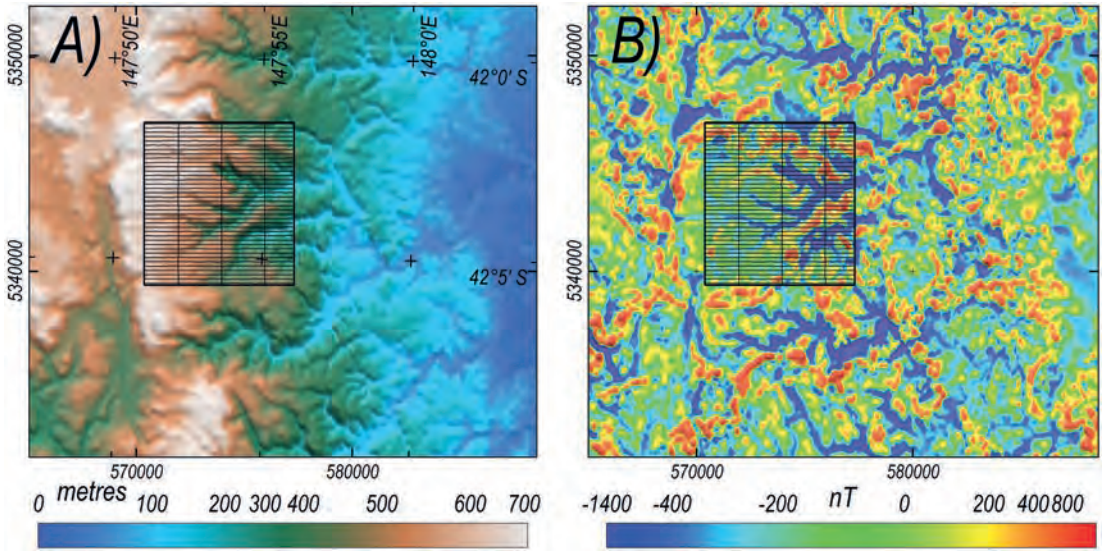


**Fig. 13.3.** A) DEM and B) TMI images of a section of the survey area over the Lost Falls Forest Reserve.

relatively homogeneous. Many surrounding areas have more pronounced magnetic highs, possibly marking individual plugs or volcanic feeders. Across the inversion area the DEM has a 390 m range from 206 to 596 m with a mean of 471 m. This surface is mapped from radar altimeter data and over the highly vegetated area these data may include some returns from the tree canopy. Over the rugged survey area it is impractical and undesirable to maintain a constant terrain clearance in flying the survey. For data continuity between adjacent

flightlines a smooth drape surface is superior. The radar elevation values measuring distance above ground vary from 48 to 197 m with an average of 90 m. We use the DEM grid to generate the top surface of a terrain model and the base surface of the excavation model.

Figure 13.4 shows the magnetisation models used in this study. Figure 13.4A is a terrain magnetisation model generated with a horizontal base and a top surface tessellated from the terrain grid. For this model we selected an initial magnetisation estimate parallel to the local geomagnetic field of declination 15.5° and inclination −72.6°. We then ran inversions to adjust the intensity and direction of magnetisation and the base level and slopes of the background regional field. The optimum magnetisation found by the inversions was 2.7 A/m, declination 73.4° and inclination −68.5°. This direction is 19° from the geomagnetic field and starting model direction, with an inclination 4° shallower than the field. The inclination of remanent magnetisation reported by Irving from remanent magnetisation measurements on samples from the nearby palaeomagnetic site was 11° steeper than our model resultant-magnetisation direction, but the model-estimated declination of resultant-magnetisation of 73° is only 5° different.

In magnetic field inversions the primary trade-off against magnetisation direction is the horizontal position of the magnetisation. However, in this study both the horizontal and vertical position of the magnetisation are locked in place by constraint of the terrain model. In running the inversions there is limited sensitivity to local features in the measured magnetic field because these effects tend to cancel over the complete model. We believe that the inversion model provides a reasonable estimate of resultant magnetisation across the volume of ground investigated. However, there are likely to be substantial local departures in intensity of magnetisation due to local inhomogeneities in the sheet, consistent with the palaeomagnetic and rock magnetic studies of Jaeger and Joplin (1954), Irving (1956, 1963), Schmidt (1976), Schmidt and McDougall (1977) and Leaman (2002). There may also be extreme local magnetisations resulting from lightning strikes, although the ground clearance of the magnetic field measurements attenuates the expression of those magnetisations substantially.

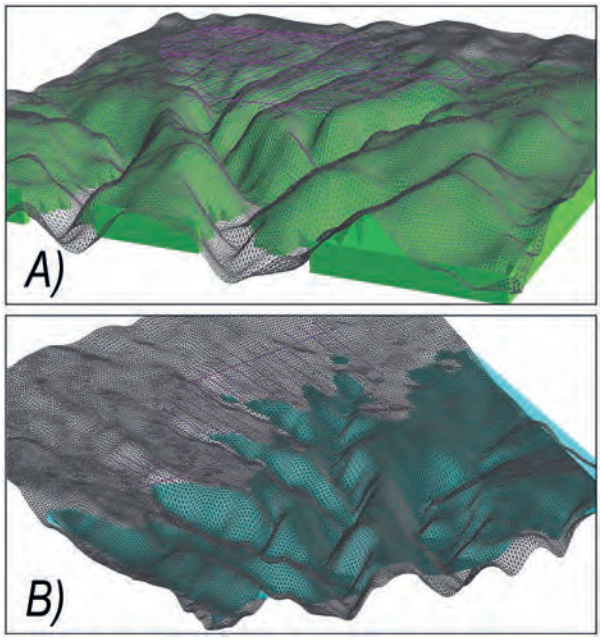


**Fig. 13.4.** A) terrain model with a tessallated top derived from the DEM grid and a horizontal base and B) an excavation model of the space between a horizontal top surface and the terrain base.

The close fit between input measured TMI and TMI forward computed from the inversion model is shown in Fig. 13.5B and an example model cross-section (the north–south tie line 190260 located in Fig. 13.5) is plotted in Fig. 13.6. Coincidence of the peaks and troughs of measured and model-computed TMI is controlled by the magnetisation direction because the model is locked in place by constraint of the terrain data. Imperfections in matching the input data are primarily misfits in amplitudes of individual peaks and troughs. These misfits could be reduced with local adjustments of the model magnetisation, particularly towards its top surface. However, such local adjustments would be mostly cosmetic and unlikely to significantly improve reliability of the bulk magnetisation estimate.

Figure 13.4B shows the alternative excavation model of the magnetisation removed from the sheet by erosion of the valleys. This model has a horizontal top and its tessellated base is generated from the terrain grid. This excavation model of free-space fits with the terrain model to create a volume bounded by a horizontal top and base, the edges of which are sufficiently removed from the field measurements that they do not cause field variations within the region of computation. We cannot use the excavation model to directly invert the measured data because, as shown in Fig. 13.6, the survey was flown on a tight drape for this rugged area and in the valleys the sensor elevation passes within the volume of the excavation model. The significant differences in sensor elevation across the region prevent reliable upward

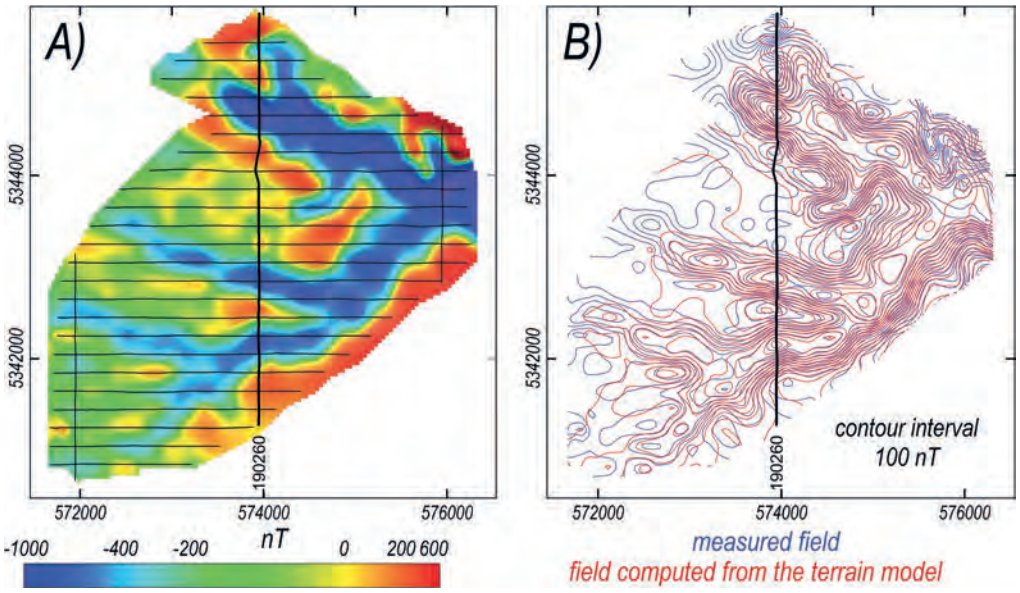


**Fig. 13.5.** A) measured TMI and B) contours of measured TMI (in blue) and TMI computed from the terrain model (in red).

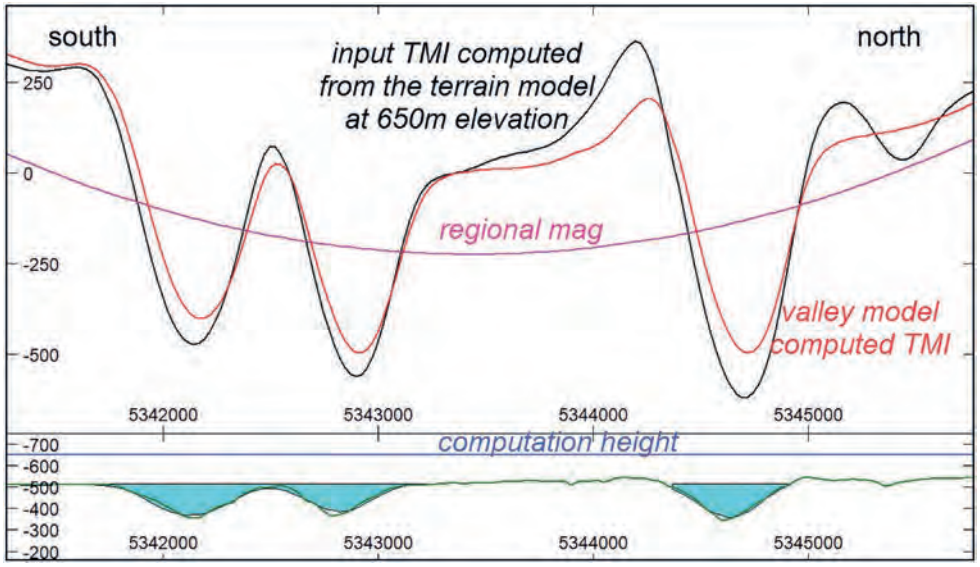


**Fig. 13.6.** Example south to north tie-line through the terrain model.

continuation of the data and the TMI grid required for upward continuation is itself is of questionable validity given this range of measurement elevation. For this study, since we had a close representation of the field along the flightlines from the terrain model computations (derived using the sensor elevation channel) we were able to use that model as an equivalent source to re-compute the field above and outside the volume of our excavation model. For this we chose a constant elevation just above terrain. This vertical translation to a virtual measurement set would not have been necessary if the survey aircraft had not flown below the top of the basalt sheet. Because in this case we used the terrain model as an intermediate step to generate the dataset for the excavation-model inversion, the excavation model cannot improve on the magnetisation estimate derived from the terrain model. We do, however, have the considerable advantage that we know the input magnetisation that the excavation-model inversion should replicate.

Figure 13.7 shows the same north–south tie-line as imaged in the lower-elevation terrain-model inversion in Fig. 13.6, with the field recomputed at a constant elevation of 650 m. Inversion of this data has an easier task than the initial inversion of the terrain model because the greater separation from the magnetisation at the higher elevation supresses some of the detail measured at the lower elevation, and because the input data is computed from a homogeneous-magnetisation model. Nevertheless, there are still imperfections in matching the two models with their different regional background fields. Figure 13.8A shows the field forward computed from the excavation model and Fig. 13.8B shows the close match between the computed fields of both the terrain model and the excavation model. The best estimate of apparent (contrast) magnetisation of the excavation model is intensity 5.03 A/m, declination 233° and inclination +72°. This magnetisation is 173° (rather than the ideal 180°) different to the input terrain model magnetisation. The discrepancy of 7° compared to the difference of 19° between the terrain-model magnetisation and the geomagnetic field direction gives us confidence that if

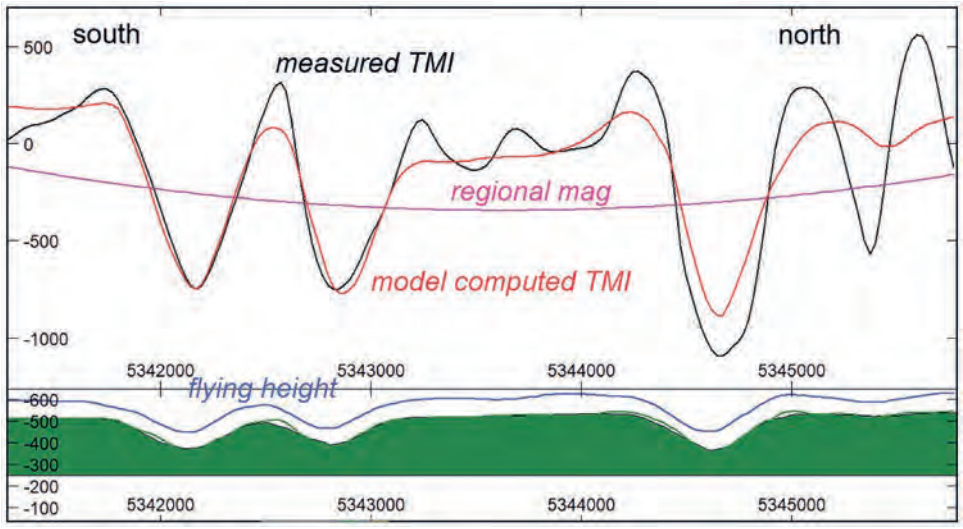


**Fig. 13.7.** Excavation model cross-section along south to north tie line 190260. The base of the model is derived from the DEM grid, the top surface is horizontal and the magnetisation is inverted from the computed field of the terrain model.

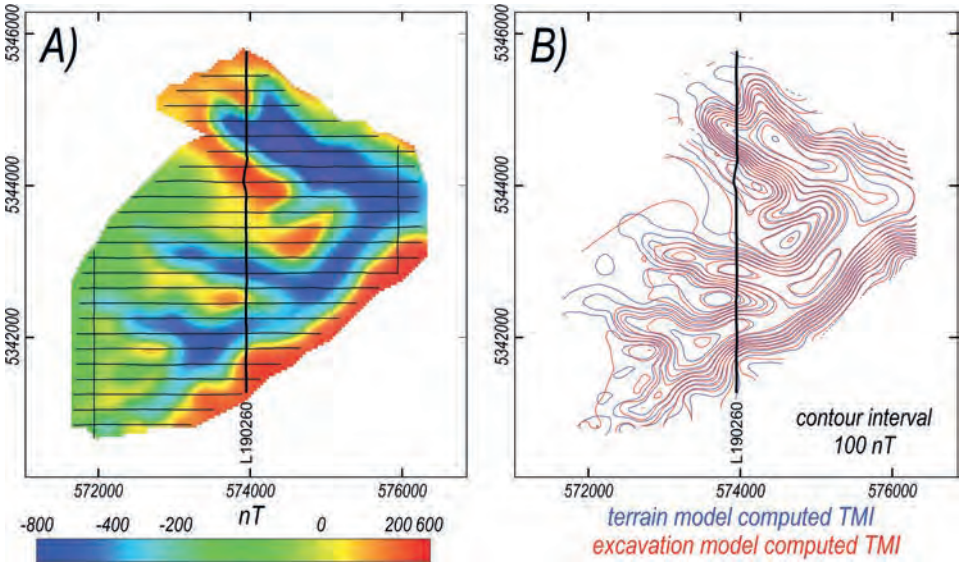


**Fig. 13.8.** A) TMI forward computed from the terrain model at a constant elevation of 650 m and B) contours of that input field (in blue) and the field computed from the inverted excavation model (in red).

the survey had been flown higher and we could have derived the excavation model directly from inversion of that measured data, that we would most likely have come to the same conclusion that the resultant-magnetisation includes expression of a steep-inclination easterly directed remanent magnetisation.

## 13.3 SYNTHETIC MAGNETIC MODELLING OF A MARTIAN IMPACT CRATER

The methodology of modelling excavation magnetic anomalies in south-east Tasmania may be suitable for future surface exploration of Mars, particularly for investigation of crustal magnetisation surrounding small impact craters. We anticipate that a terrain model is likely to be the starting point for magnetic field modelling of these small craters and that complexity will only be added if that initial model proves inadequate. To test our ability to recover the crustal magnetisation surrounding an impact crater we selected a simple crater of approximately 8 km diameter from the Mars MGS MOLA DEM (version 2) measured by the Mars Orbital Laser Altimeter (Smith *et al.* 2001) flown on the Mars Global Surveyor spacecraft (Albee *et al.* 2001) and processed by Neumann *et al.* (2001) and Neumann *et al.* (2003). The location of the crater is shown in Fig. 13.9 and the terrain variation is imaged in Fig. 13.10A. The depth of the crater is ~800 m with a depth to diameter ratio of 0.1. This particular crater has only a minor rim that does not require independent treatment in the modelling. We assume that the crater wall is the bounding surface of a magnetisation that is homogeneous at the crater scale. For surface exploration on Mars we anticipate that greater use could be made of smaller features, but this 8 km diameter crater allows us to generate an acceptable terrain model from the available 463 m cell size grid. In any surface exploration we expect that a more detailed terrain grid would be available for magnetic field modelling. As already mentioned, there is a constant amplitude of magnetic field variations for surveys with measurement elevation and extent proportional to model size, so our findings are size independent.

Figure 13.10A shows the terrain grid over the chosen impact crater and Figs 13.10B and 13.10C show two total magnetic intensity (TMI) images computed by assigning different magnetisations to the model generated from that grid. There is a difference of 116° between these two magnetisation directions but it is challenging to predict those directions from the TMI anomalies. On Earth, anomalous magnetic fields sum with the background field to in some places reinforce it giving positive TMI features and in other places oppose it giving negative TMI features. With experience of magnetic fields measured in a particular geomagnetic inclination the approximate magnetisation direction of compact anomalies can be predicted by visual inspection (see Chapter 5) but on

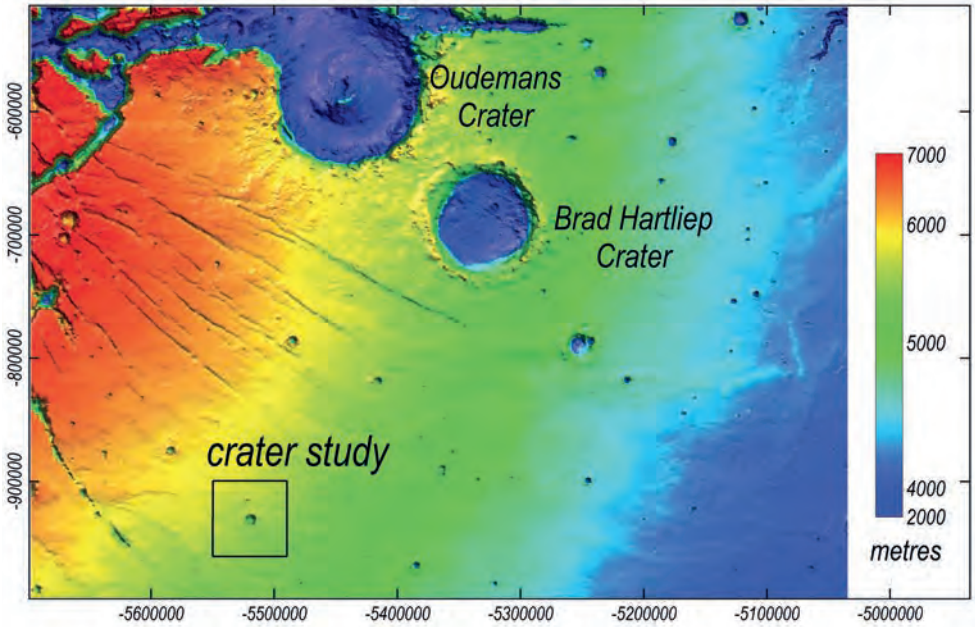


**Fig. 13.9.** Martian terrain model detail from the MARS MGS MOLA DEM (version 2) showing the location of the crater selected for study.

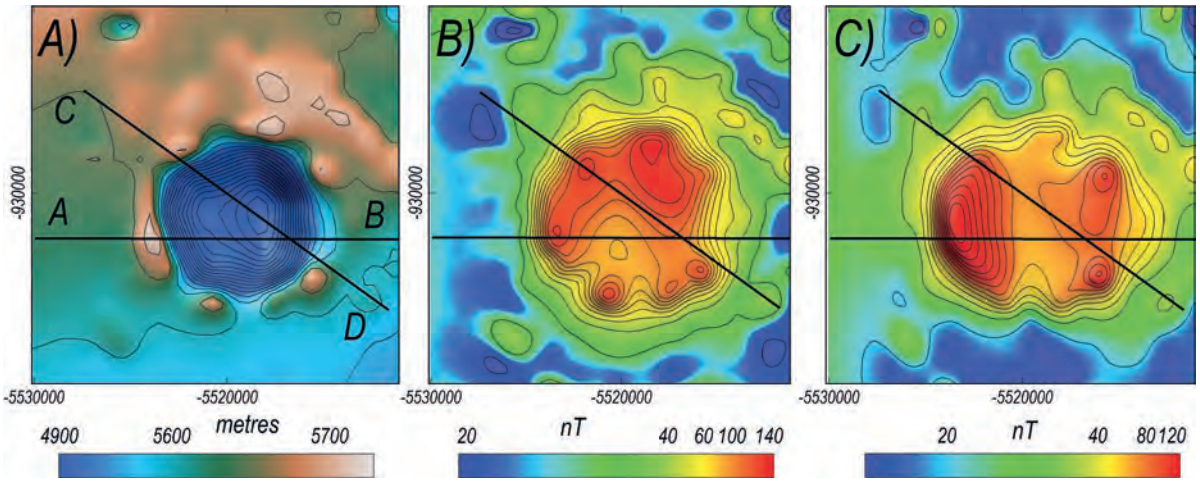


**Fig. 13.10.** A) terrain image of the selected crater and B) and C) TMI anomalies over the crater for magnetisations in the surrounding crust of B) declination 0°, inclination −60° and C) declination 90°, inclination +30° respectively.

Mars in a very weak background field TMI anomalies are almost universally positive-only and their pattern is less diagnostic of magnetisation direction. In Chapter 16 we discussed the advantages of multicomponent vector data for magnetic field studies in weak background fields and those advantages also apply to excavation anomalies. Figure 13.11 shows images of the three orthogonal vector component anomalies corresponding to the TMI anomalies in Figs 13.10B and 13.10C. For Martian surface exploration it may be impractical to make sufficient measurements to obtain such imagery but we can use these images to understand the component variations along the two profiles shown, and the multi-component data on those two profiles is sufficient to resolve the surrounding magnetisation. For the steep inclination (–60°) magnetisation A in the top row of Fig. 13.11 the two horizontal components show dipole anomalies of similar positive and negative amplitudes. The vertical component is predominantly positive and maps the crater extents more conveniently. Note that the polarity of $B_z$ is opposite to that of the magnetisation because the crater is a deficit magnetisation. For the less steep magnetisation B with an inclination of +30° shown in the lower row of Fig. 13.11, the $B_z$ component is mixed polarity but

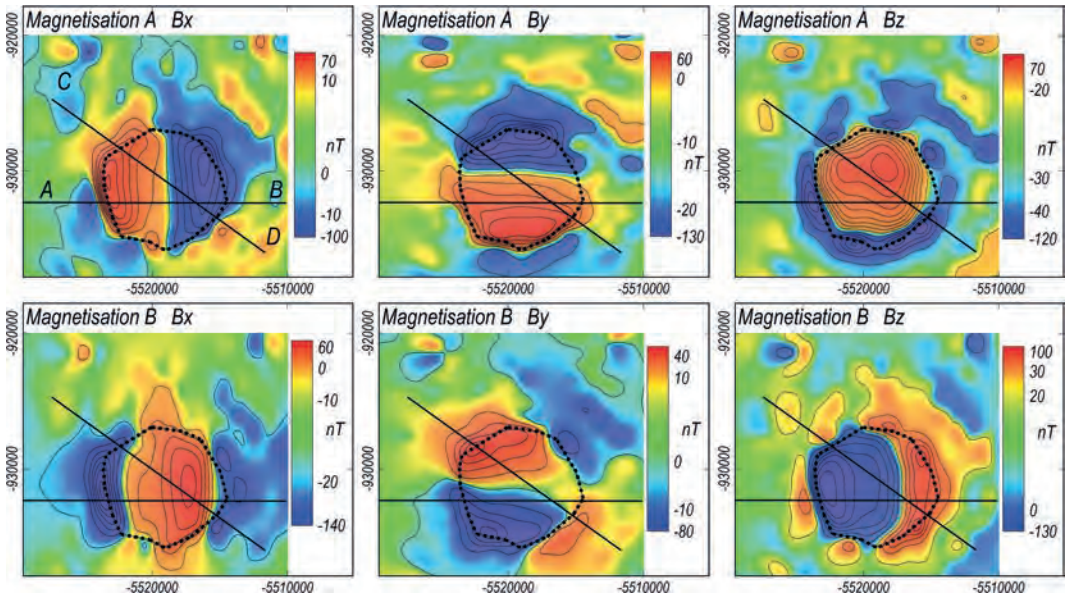


**Fig. 13.11.** Magnetic field Bx, By, Bz component anomalies over the crater (with dashed outline) for surrounding magnetisations A) declination 0°, inclination −60° (top row) and B) declination 90°, inclination +30° (bottom row).

with dominant polarity also opposite to that of the magnetisation. The horizontal $B_x$ component parallel to the northerly declination of this magnetisation produces a prominent positive anomaly and the horizontal $B_y$ component perpendicular to the magnetisation produces a weaker quadrupole anomaly.

Figure 13.12A shows the terrain model from which the component grids and profiles in Fig. 13.11 were computed and Fig. 13.12B shows the excavation model that uses the terrain grid as its base and has a horizontal top coincident with the ground elevation around the crater. The excavation model was used to invert the profiles computed from the terrain model at an elevation of 6,000 m (360 m above its top). The inversion results are shown for the magnetisation A model in Fig. 13.13 and for the magnetisation B model in Fig. 13.14. These were multi-component inversions of both survey lines that sought to simultaneously optimise the fit to all three components on both lines. These fits do not match the details of the field computed from the more complex terrain model but for both magnetisation directions all three components show an approximate fit and this corresponds with close recovery of the input model magnetisation direction. For magnetisation A, the excavation model has a magnetisation of declination 175.6°, inclination +59.3° that gives an anti-parallel crustal magnetisation estimate of declination 355.6°, inclination −59.3° (a discrepancy of 2.3° with the input direction). For magnetisation B, the excavation model has a magnetisation of declination 269.8°, inclination −28.8° that gives an anti-parallel crustal magnetisation estimate of declination 89.8°, inclination +28.8° (a discrepancy with the input direction of 1.2°). Depending on magnetisation direction (that is unknown before the survey) a single profile may not have an orientation well suited to investigation of the magnetisation. An effective survey procedure would be to fly two profiles of different orientation as shown in Fig. 13.11. Hopefully suitable terrain features (including but not necessarily limited to impact craters) will be sufficiently common that a regional survey could step from one feature to the next.

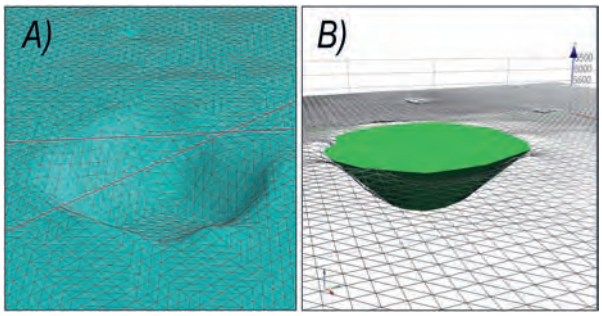


**Fig. 13.12.** Alternative models of A) terrain used for forward computation of the input fields for this study and B) the space model of the crater excavation used in inversion. The model volumes have magnetisations of equal strength and opposite direction.

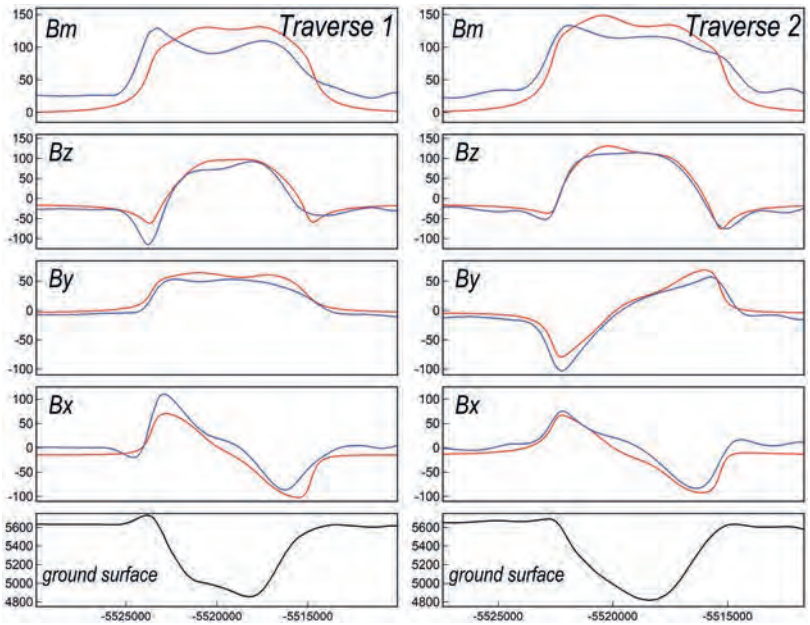


**Fig. 13.13.** Bx, By and Bz components on traverses A-B (left) and C-D (right): (blue) computed from the terrain model with magnetisation A, and (red) inverted from the excavation model.

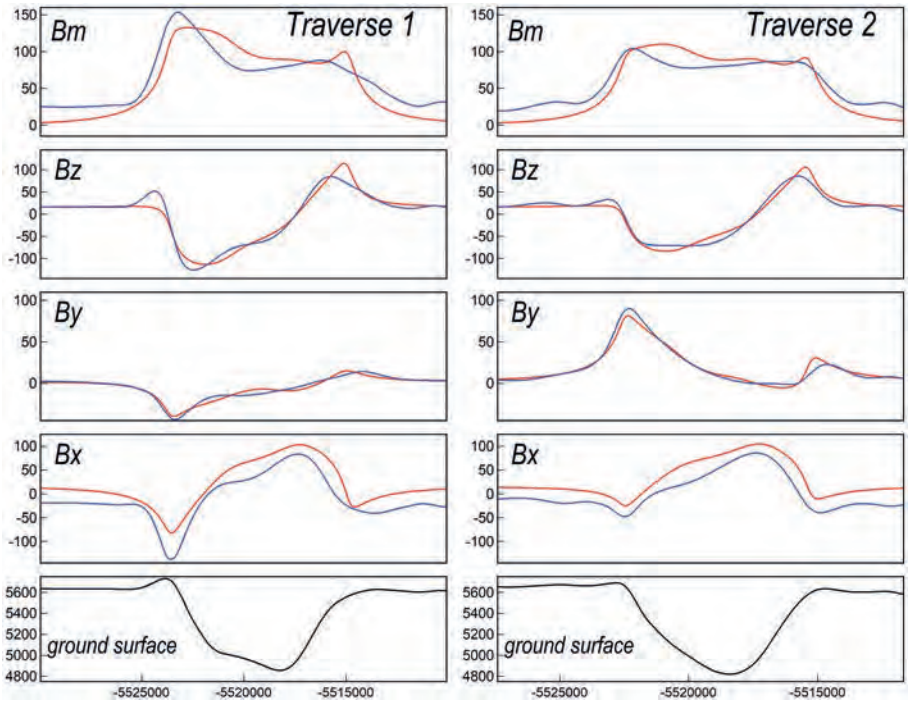


**Fig. 13.14.** Bx, By and Bz components on traverses A-B (left) and C-D (right): (blue) computed from the terrain model with magnetisation B, and (red) inverted from the excavation model.

## 13.4 SYNTHETIC MAGNETIC MODELLING OF A MARTIAN CRATER WITH DEMAGNETISATION AND IMPACT MAGNETISATION

We briefly investigate the case that the crater terrain may not be the key bounding surface for crustal magnetisations if there is surrounding demagnetisation caused by the impact. From the crater morphology the expected distributions of stress and temperature generated by the impact can be inferred (Mohit and Arkani-Hamed 2004; Shahnas and Arkani-Hamed 2007) but without knowledge of the pre-impact magnetisation or rock magnetic properties it is not feasible to predict the post-impact magnetisation. We investigate separate cases that an impact into a magnetised crust during a period when the magnetic field is weak or non-existent excavates a crater and causes demagnetisation beneath and surrounding it. In a further example we consider the case that an impact during a period when the magnetic field is strong into a crust that is initially weakly magnetic or non-magnetic excavates a crater and generates an annulus of strong magnetisation around it with a remanent magnetisation acquired on cooling from the impact-generated heating event. These simple conceptual models illustrate aspects of the magnetic field that might be investigated with advantage in mapping crustal magnetisation.

Figure 13.15 illustrates two east–west multi-component magnetic field profiles acquired at 50 m and 1,000 m above an impact crater for which demagnetisation doubles the depth of missing magnetisation. The crust is assigned a pre-crater, mid-inclination magnetisation with declination 45° and inclination +45°. To model this scenario we create a model of missing magnetisation (either through excavation or demagnetisation) reverse to the crustal magnetisation with declination 225° and inclination −45°. The dashed curves in Fig. 13.15 show the magnetic field computed for the magnetisation contrast due to the excavated crater and the solid curves show the field for the contrast of the crater plus the surrounding demagnetised zone. The crater diameter is 5,000 m, the depth is 500 m and the demagnetisation extends to another 500 m depth. Both curves have similar patterns for each of all the three components, revealing that the additional demagnetisation zone would not cause any significant difference in estimated magnetisation direction. An optimum inversion fit using the crater model would result in overestimation of the intensity of crustal magnetisation as a result of the excluded volume of magnetisation lost in

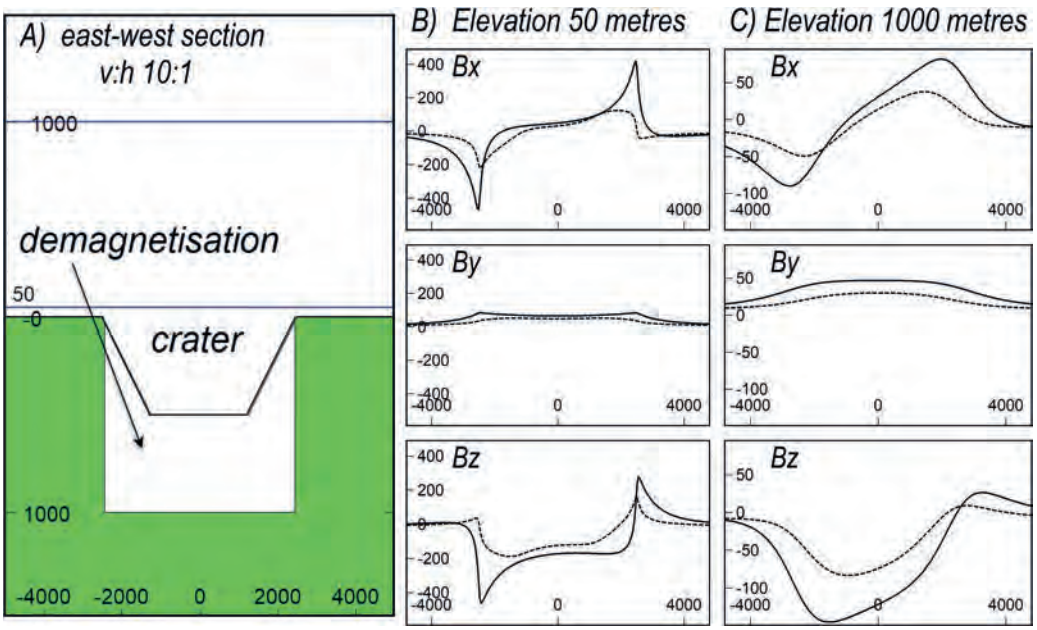


**Fig. 13.15.** A) 5 km diameter 500 m deep crater with impact demagnetisation extending to an additional depth of 500 m, with a west to east traverse at elevations B) 50 m and C) 1 km. Dashed line for the crater only, solid line for the crater and demagnetised zone.

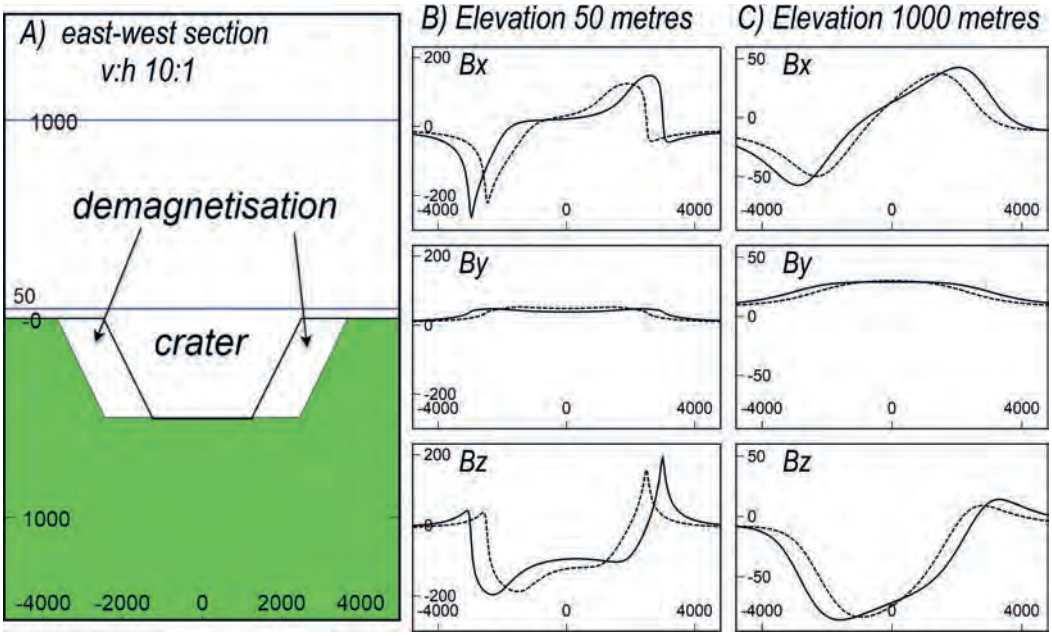


**Fig. 13.16.** A) Model of a 5 km diameter 500 m deep crater with impact demagnetisation extending 500 around it and magnetic components computed on an east–west traverse at B) elevation of 50 m and C) elevation of 1 km.

the demagnetisation zone. There would be a significant post-inversion data-misfit because the deeper demagnetisation zone has a broader and less sharp magnetic field expression than the shallower crater. This discrepancy is most noticeable in the lower elevation profile (Fig. 13.15B). A discrepancy with the terrain model might occur if the crater is infilled with transported material or chaotic blocks of random orientation that have a low bulk intensity of remanent magnetisation.

Figure 13.16 shows a model where demagnetisation surrounds the crater. As with demagnetisation beneath the crater, demagnetisation around it also increases the amplitude of the magnetic field variations, but in this case the most prominent change to the anomaly is its

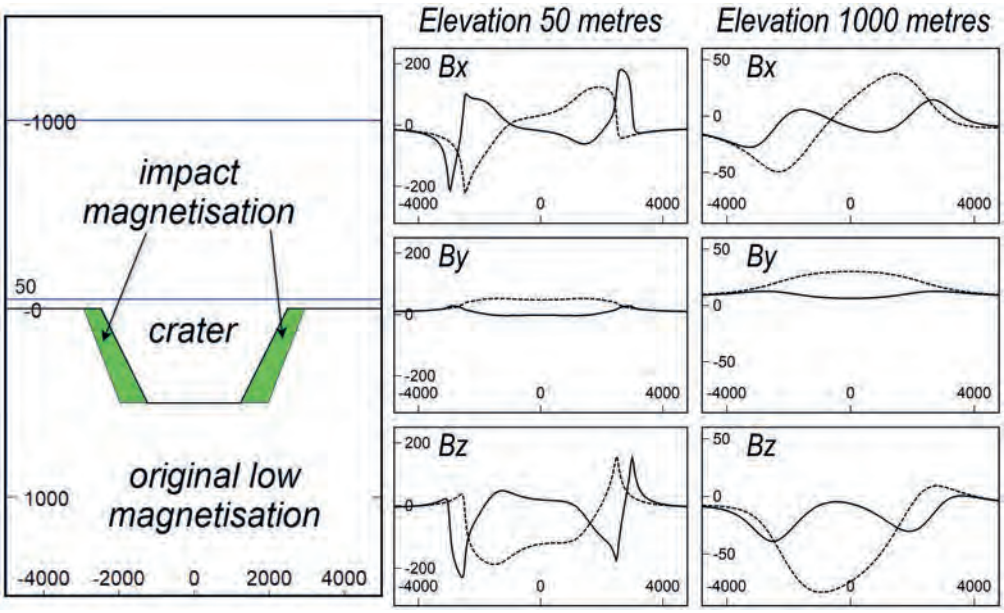


**Fig. 13.17.** Model with impact magnetisation (in green) extending 500 m around the crater, with magnetic components computed on an east–west traverse at elevations of B) 50 m and C) 1 km. The dashed lines from Figs 13.15 and 13.16 are shown for comparison only.

increased width, with outward migration of the anomaly peaks and troughs from the crater wall to the more distant edge of demagnetisation. The expression of demagnetisation both beneath and around the crater is most evident in the lower elevation measurements. For all three components, at both elevations, peak and trough amplitude ratios of the crater anomalies with and without demagnetisation are broadly similar, giving similar estimates of magnetisation directions. Given the additivity of magnetic fields, combined demagnetisation both around and beneath the crater (with possible error in estimation of its volume) is expected to mostly impact on estimation of the strength of the surrounding magnetisation.

Figure 13.17 shows another simplified concept model where impact into an initially non-magnetic crust occurs during a period of a strong background field. Excavation of the crater does not cause a magnetisation contrast with the originally non-magnetic crust, but a zone of thermo-remanent magnetisation (TRM) is created where the surrounding crust heated by the impact then cools through the blocking temperature of its ferromagnetic minerals. This model of an annular magnetisation surrounding the crater is only marginally more complex than the first two cases we investigated. In the impact magnetisation model of Fig. 13.17 the crater has the same zero magnetisation as the background crust and would not be magnetically visible except for the annulus of magnetisation surrounding it. In this example we gave the new, annular magnetisation a magnetisation with declination 225° and inclination −45°. This is the same magnetisation direction as the contrast magnetisation for the crater in the previous examples, but the magnetic anomalies are quite different because the annulus magnetisation (20% of the crater diameter) also has an external contact. If the anomaly is well defined it should be straightforward to discriminate between an annular magnetisation surrounding a crater and basement magnetisation extending well beyond it. Figures 13.17B and 13.17C show that the zone of annular magnetisation is most obvious at lower levels. At substantially greater elevations the magnetic field expressions from both sides of the crater overlap and lose their diagnostic characteristics.

We have investigated the case only of impact-induced magnetisation of a previously un-magnetised basement but provided the measurement field extends sufficiently beyond the annular zone it should be possible to individually resolve differently directed (more than ~30° difference) extensive pre-impact and local circum-crater impact-caused magnetisations, even though there is likely to be extensive transition and overlap between them. Nevertheless, this two-magnetisation case (three magnetisations including the zero magnetisation of the crater) is more complex than the single-contrast magnetisations considered previously and would require

favourable conditions of strong magnetisations and high-resolution measurements to recover reliable estimates of the magnetisation directions.

## 13.5 CONCLUSIONS

We have shown both with modelling and inversion of measured TMI anomalies over valleys incised into sheets of the Tasmanian dolerites, and with synthetic modelling and inversion of vector component data computed from the terrain model of a Martian impact crater, that a model of excavated magnetisation can be used to emulate sheets of magnetisation complete other than for that excavation. The surrounding material is then assigned a magnetisation of equal strength and opposite polarity to the removed magnetisation. This method of modelling and inversion has the advantage that models are more compact than would be required to represent the surrounding magnetisation. We hope that with future developments of magnetic surveying on Mars this approach may be of benefit in deriving bulk magnetisation estimates for materials surrounding small impact craters.

## REFERENCES


Albee AL, Arvidson RE, Palluconi F, Thorpe T (2001) Overview of the Mars Global Surveyor mission. *Journal of Geophysical Research* **106**(E10), 23291–23316. doi:10.1029/2000JE001306

Arkani-Hamed J (2005) Magnetic crust of Mars. *Journal of Geophysical Research* **110**, E08005. doi:10.1029/2004JE002397

Brauns CM, Hergt JM, Woodhead JD, Maas R (2000) Os isotopes and the origin of the Tasmanian Dolerites. *Journal of Petrology* **41**, 905–918. doi:10.1093/petrology/41.7.905

Hergt JM, Brauns CM (2001) On the origin of Tasmanian dolerites. *Australian Journal of Earth Sciences* **48**, 543–549. doi:10.1046/j.1440-0952.2001.00875.x

Irving E (1956) The magnetisation of the Mesozoic dolerites of Tasmania. *Papers and Proceedings of the Royal Society of Tasmania* **90**, 157–168. doi:10.26749/VKVI2019

Irving E (1963) Paleomagnetism of the Narrabeen chocolate shale and the Tasmanian dolerite. *Journal of Geophysical Research* **68**, 2283–2287. doi:10.1029/JZ068i008p02283

Jaeger JC, Joplin G (1954) Rock magnetism and the differentiation of dolerite sill. *Journal of the Geological Society of Australia* **2**(1), 1–19. doi:10.1080/00167615408728454

Leaman D (2002) The effective magnetisation of the Jurassic dolerites of Tasmania. *Exploration Geophysics* **33**, 166–171. doi:10.1071/EG02166

Lillis RJ, Robbins S, Manga M, Halekas JS, Frey HV (2013) Time history of the Martian dynamo from crater magnetic field analysis. *Journal of Geophysical Research* **118**, 1488–1511. doi:10.1002/jgre.20105

Louzada KL, Stewart ST, Weiss BP, Gattacceca J, Lillis RJ, Halekas JS (2011) Impact demagnetization of the martian crust: current knowledge and future directions. *Earth and Planetary Science Letters* **305**, 257–269. doi:10.1016/j.epsl.2011.03.013

Mittelholz A, Johnson CL, Feinberg JM, Langlais B, Phillips RJ (2020) Timing of the martian dynamo: New constraints for a core field 4.5 and 3.7 Ga ago. *Science Advances* **6**, 1–7.

Mohit PS, Arkani-Hamed J (2004) Impact demagnetization of the Martian crust. *Icarus* **168**, 305–317. doi:10.1016/j.icarus.2003.12.005

Neumann GA, Rowlands DD, Lemoine FG, Smith DE, Zuber MT (2001) Crossover analysis of Mars Orbiter Laser Altimeter data. *Journal of Geophysical Research* **106**(E10), 23753–23768. doi:10.1029/2000JE001381

Neumann GA, Smith DE, Zuber MT (2003) Two Mars years of clouds detected by the Mars Orbiter Laser Altimeter. *Journal of Geophysical Research* **108**(E4), 5023. doi:10.1029/2002JE001849

Robbins SJ, Hynek BM (2012) A new global database of Mars impact craters ≥ 1 km: 2 Global crater properties and regional variations of the simple-to-complex transition diameter. *Journal of Geophysical Research* **117**, E06001. doi:10.1029/2011JE003967

Schmidt PW (1976) The non-uniqueness of the Australian Mesozoic palaeomagnetic pole position. *Geophysical Journal of the Royal Astronomical Society* **47**, 285–300. doi:10.1111/j.1365-246X.1976.tb01274.x

Schmidt PW, McDougall I (1977) Palaeomagnetic and potassium-argon dating studies of the Tasmanian dolerites. *Journal of the Geological Society of Australia* **24**, 321–328. doi:10.1080/00167617708728991

Shahnas H, Arkani-Hamed J (2007) Viscous and impact demagnetization of Martian crust. *Journal of Geophysical Research* **112**, E02009. doi:10.1029/2005JE002424

Smith DE, Zuber MT, Frey HV, Garvin JB, Head JW, Muhleman DO, Pettengill GH, *et al*. (2001) Mars Orbiter Laser Altimeter—Experiment summary after the first year of global mapping of Mars. *Journal of Geophysical Research* **106**, 23689–23722. doi:10.1029/2000JE001364

Vervelidou F, Lesur V, Grott M, Morschhauser A, Lillis RJ (2017) Constraining the date of the martian dynamo shutdown by means of crater magnetization signatures. *Journal of Geophysical Research* **122**, 2294–2311. doi:10.1002/2017JE005410